

## PHYSICS

## Holography and criticality in matchgate tensor networks

A. Jahn<sup>1\*</sup>, M. Gluza<sup>1</sup>, F. Pastawski<sup>1</sup>, J. Eisert<sup>1,2,3</sup>

The AdS/CFT correspondence conjectures a holographic duality between gravity in a bulk space and a critical quantum field theory on its boundary. Tensor networks have come to provide toy models to understand these bulk-boundary correspondences, shedding light on connections between geometry and entanglement. We introduce a versatile and efficient framework for studying tensor networks, extending previous tools for Gaussian matchgate tensors in 1 + 1 dimensions. Using regular bulk tilings, we show that the critical Ising theory can be realized on the boundary of both flat and hyperbolic bulk lattices, obtaining highly accurate critical data. Within our framework, we also produce translation-invariant critical states by an efficiently contractible tensor network with the geometry of the multiscale entanglement renormalization ansatz. Furthermore, we establish a link between holographic quantum error-correcting codes and tensor networks. This work is expected to stimulate a more comprehensive study of tensor network models capturing bulk-boundary correspondences.

## INTRODUCTION

The notion of holography in the context of bulk-boundary dualities, most famously expressed through the anti-de Sitter space/conformal field theory (AdS/CFT) correspondence (1), has had an enormously stimulating effect on recent developments in theoretical physics. A key feature of these dualities is the relationship between bulk geometry and boundary entanglement entropies (2–4), prominently elucidated by the Ryu-Takayanagi formula (5). Because of the importance of entanglement in the context of AdS/CFT (6), it was quickly realized that tensor networks are ideally suited for constructing holographic toy models, most notably the multiscale entanglement renormalization ansatz (MERA) (7–9). The realization that quantum error correction could be realized by a holographic duality (10) further connected to ideas from quantum information theory. Despite the successful construction of several tensor network models that reproduce various aspects of AdS/CFT [see, e.g., (11–13)], a general understanding of the features and limits of tensor network holography is still lacking. Particular obstacles are the potentially large parameter spaces of tensor networks and the considerable computational cost of contraction.

In this work, we overcome some of these challenges by applying highly efficient contraction techniques developed for matchgate tensors (14, 15), which replace tensor contraction by a Grassmann-variate integration scheme. These techniques allow us to comprehensively study the interplay of geometry and correlations in Gaussian fermionic tensor networks in a versatile fashion, incorporating toy models for quantum error correction and tensor network approaches for CFT, such as the MERA, into a single framework, highlighting the connections between them. Furthermore, this framework includes highly symmetrical tensor networks based on regular tilings (see Fig. 1, A and B). We are thus in a position to efficiently probe the full space of Gaussian bulk-boundary correspondences from a small set of parameters, including the bulk curvature. We show that matchgate tensor networks with a variety of bulk geometries contain the Ising CFT in their parameter space to remarkably good approximation as a special

case, with properties similar to the wavelet MERA model (16, 17). While regular hyperbolic tilings have recently been considered as a MERA alternative (18), we show that flat tilings can lead to very similar boundary states. In our studies, we restrict ourselves to tensor networks that are nonunitary and real, resembling a Euclidean evolution from bulk to boundary. In particular, we do not require the causal constraints of the MERA for efficient contraction, thus providing new approaches in the context of tensor network renormalization (19, 20). While we provide substantial evidence that tensor networks are capable of describing bulk-boundary correspondences beyond known models and introduce a framework for their study, our work is by no means exhaustive. We do hope to provide a starting point for more systematic studies of holography in tensor networks.

## MATERIALS AND METHODS

We constructed two-dimensional planar tensor networks with fermionic bulk and boundary degrees of freedom. The bulk degrees of freedom are associated with a set  $V$  of vertices of a tensor network. At each vertex,  $v \in V$ , a local tensor  $T_v$  with  $k_v$  indices is placed, which can be interpreted as a local fermionic state on  $k_v$  sites. After contraction over all connected bulk indices, the  $L$  remaining open indices are interpreted as boundary sites with the boundary state specified by the full contracted tensor. Because of the planarity of the network, the boundary sites form a loop. The bulk geometry can be flat or negatively curved (a positively curved network closes in on itself after finite distance). We visualized our tensor networks by representing each tensor  $T_v$  as a  $k_v$ -gon whose edges correspond to indices. Thus, the tensor network is represented by a polygon tiling, which determines the bulk geometry. Adjacent edges between two polygons correspond to contracted indices and boundary edges to open ones. See Fig. 1 for examples.

Concretely, each bulk degree of freedom  $v \in V$  is associated with a local tensor  $T_v: \{0,1\}^{\times r} \rightarrow \mathbb{C}$  of tensor rank  $r$  (equal to the number of edges of the corresponding tile), all of which are contracted to form tensors of higher rank. We denote the tensor component at indices  $j \in \{0,1\}^{\times r}$  as  $T_v(j)$  and the standard computational basis for  $r$  boundary spins as  $|j\rangle := \otimes_{k=1}^r |j_k\rangle$ . Each tensor is then equivalent to a state vector

$$|\psi_v\rangle = \sum_{j \in \{0,1\}^{\times r}} T_v(j) |j\rangle \quad (1)$$

<sup>1</sup>Dahlem Center for Complex Quantum Systems, Freie Universität Berlin, 14195 Berlin, Germany. <sup>2</sup>Helmholtz-Zentrum Berlin für Materialien und Energie, 14109 Berlin, Germany. <sup>3</sup>Department of Mathematics and Computer Science, Freie Universität Berlin, 14195 Berlin, Germany.

\*Corresponding author. Email: a.jahn@fu-berlin.de

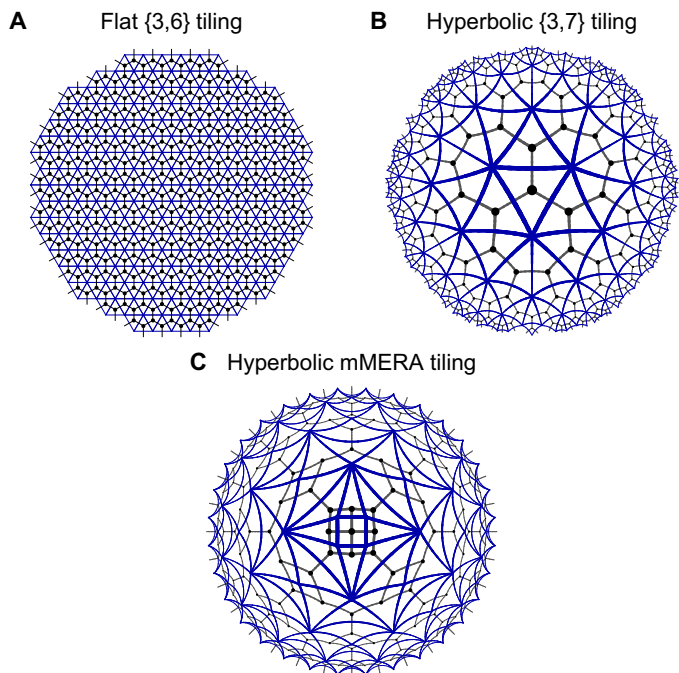


**Fig. 1. Geometries of tensor networks.** Discretizations of flat (A) and hyperbolic space (B and C) with a triangular tiling (blue edges), into which a tensor network is embedded (black lattice). In the matchgate formalism, joint edges between triangles correspond to an integration over a pair of Grassmann numbers, analogous to tensor network contraction over indices. While (A) and (B) show regular tilings, (C) presents a nonregular MERA-like tiling we call the matchgate MERA (mMERA).

For a broader introduction to tensor networks and their contractions, see (21–24).

Instead of explicit tensor contraction along pairs of indices, we used the formalism from (15) using Grassmann integration. Any tensor  $T$  can be represented by a Grassmann-variate characteristic function

$$\Phi_T(\theta) = \sum_{j \in \{0,1\}^{\times r}} T(j) \theta_1^{j_1} \theta_2^{j_2} \dots \theta_r^{j_r} \quad (2)$$

where the  $\theta_k$  are Grassmann numbers defined by the anticommutation relation  $\theta_k \theta_{k'} + \theta_{k'} \theta_k = 0$ . The contraction  $T_{1*2}$  of two tensors  $T_1$  and  $T_2$  (of rank  $r_1$  and  $r_2$ , respectively) over the last index of  $T_1$  and the first index of  $T_2$  is given by

$$T_{1*2}(x, y) = \sum_{z \in \{0,1\}} T_1(x, z) T_2(z, y) \quad (3)$$

where  $x \in \{0,1\}^{\times(r_1-1)}$ ,  $y \in \{0,1\}^{\times(r_2-1)}$ .  $T_{1*2}$  has rank  $r_1 + r_2 - 2$ . The characteristic function of the contraction is obtained as

$$\Phi_{T_{1*2}}(\xi) = \int d\eta_1 \int d\theta_{r_1} \Phi_{T_1}(\theta) \Phi_{T_2}(\eta) \exp(\theta_{r_1} \eta_1) \quad (4)$$

where we used  $\xi = (\theta_1, \dots, \theta_{r_1-1}, \eta_2, \dots, \eta_{r_2})$  and  $\int d\eta_1 \int d\theta_{r_1}$  denotes Grassmann integrals, anticommuting multilinear functionals obeying  $\int d\xi_j \xi_j^{z_j} = \delta_{z_j,1}$  [see (15, 25–27) for more details]. A self-contained derivation of the equivalence of (4) with tensor contraction, as well as a note on iterated integrals, is given in the Supplementary Materials. Anticommutativity requires an appropriate labeling of all Grassmann

variables, but such a labeling can always be found for contractions of planar networks (15). These Grassmann integrations are particularly efficient to compute for the case of matchgate tensors, where their computation scales polynomially in the number of tensor indices.

Consider a rank  $r$  tensor  $T(x)$  with inputs  $x \in \{0,1\}^{\times r}$ . One calls  $T(x)$  a matchgate if there exists an antisymmetric matrix  $A \in \mathbb{C}^{r \times r}$  and a  $z \in \{0,1\}^{\times r}$  so that one can write

$$T(x) = \text{Pf}(A_{|x \text{ XOR } z}) T(z) \quad (5)$$

where  $\text{Pf}(A)$  is the Pfaffian of  $A$  and  $A_{|x}$  is the principal submatrix of  $A$  acting on the subspace supported by  $x$ . Furthermore, one calls  $T(x)$  an even tensor if  $T(x) = 0$  for any  $x$  with odd  $\sum_j x_j$ .

A generic even matchgate has a simple Gaussian characteristic function of the form

$$\Phi_T(\theta) = T(0) \exp\left(\frac{1}{2} \sum_{j,k=1}^r A_{j,k} \theta_j \theta_k\right) \quad (6)$$

where  $T(0)$ , the tensor component for all-zero input, acts as a normalization factor. Apart from normalization, the full tensor is completely determined by  $A$ , which we therefore call the generating matrix. Thus, the rules for contracting matchgate tensors can be written as rules for combining generating matrices. Full derivations of these, including the calculation of physical covariance matrices from the generating matrices, are provided in the Supplementary Materials. With our contraction rules, the computational cost of contracting two tensors is quadratic in the number of indices of the final tensor. Thus, we could bound the total computational cost for contracting an entire network of the type considered here by  $O(L^2 N)$ , where  $L$  is the number of boundary sites and  $N$  is the number of contracted tensors [for similar bounds on matchgate contraction, see (15)].

Using Pauli matrices  $\sigma^\alpha$  with  $\alpha \in \{x, y, z\}$ , one can define Majorana operators  $\gamma_i$  via the Jordan-Wigner transformation

$$\gamma_{2k-1} = (\sigma^z)^{\otimes(k-1)} \otimes \sigma^x \otimes (\mathbb{1}_2)^{\otimes(r-k)} \quad (7)$$

$$\gamma_{2k} = (\sigma^z)^{\otimes(k-1)} \otimes \sigma^y \otimes (\mathbb{1}_2)^{\otimes(r-k)} \quad (8)$$

The computational basis is then equivalent to an occupational basis. In this context, we proved that any fermionic Gaussian state vector in the form of Eq. 1 has coefficients  $T(j)$  constituting a matchgate tensor. For details on this proof, refer to the Supplementary Materials. The converse statement is also true, providing a further perspective on the connection to free fermions (28).

## RESULTS

### The holographic pentagon code

We will now apply our framework to the highly symmetric class of regular bulk tilings, first implementing the holographic error correcting code (HaPPY code) proposed in (12) and then exploiting the versatility of our framework to extend it toward more physical setups. The HaPPY code furnishes a mapping between additional (uncontracted) bulk degrees of freedom on each tensor and the boundary state, realized by a bulk tiling of pentagons. Each pentagon tile encodes

one fault-tolerant logical qubit via the encoding isometry of the five-qubit code. This  $[[5,1,3]]$  quantum error-correcting code (29) saturates both the quantum Hamming bound (30, 31) and the singleton bound (31) and can be expressed as a stabilizer code (32).

We observe that fixing the bulk degrees of freedom to computational basis states gives rise to a matchgate tensor network, as the logical computational basis states of the holographic pentagon code can be viewed as ground states of a quadratic fermionic Hamiltonian. This can be seen directly by applying Eqs. 7 and 8 onto the stabilizers  $S_k$  of the underlying  $[[5,1,3]]$  code, thus expressing it in terms of Majorana operators  $\gamma_i$  and a total parity operator  $\mathcal{P}_{\text{tot}} = (\sigma^z)^{\otimes 5}$  as

$$\begin{aligned}
 S_1 &= \sigma^x \otimes \sigma^z \otimes \sigma^z \otimes \sigma^x \otimes 1_2 = i\gamma_7\gamma_2 \\
 S_2 &= 1_2 \otimes \sigma^x \otimes \sigma^z \otimes \sigma^z \otimes \sigma^x = i\gamma_9\gamma_4 \\
 S_3 &= \sigma^x \otimes 1_2 \otimes \sigma^x \otimes \sigma^z \otimes \sigma^z = i\mathcal{P}_{\text{tot}}\gamma_6\gamma_1 \\
 S_4 &= \sigma^z \otimes \sigma^x \otimes 1_2 \otimes \sigma^x \otimes \sigma^z = i\mathcal{P}_{\text{tot}}\gamma_8\gamma_3 \\
 S_5 &= \sigma^z \otimes \sigma^z \otimes \sigma^x \otimes 1_2 \otimes \sigma^x = i\mathcal{P}_{\text{tot}}\gamma_{10}\gamma_5
 \end{aligned}
 \tag{9}$$

As the corresponding stabilizer Hamiltonian is given by  $H = -\sum_{k=1}^5 S_k$ , we find a doubly degenerate ground state whose degeneracy is lifted by the parity operator  $\mathcal{P}_{\text{tot}}$ . The resulting two states with parity eigenvalues  $\pm 1$  correspond to the logical eigenstates  $\bar{0}$  and  $\bar{1}$ , which are themselves ground states of purely quadratic Hamiltonians with different parity factors. Thus, both computational basis states are pure Gaussian, leading us to the conclusion that for fixed computa-

tional input in the bulk, the holographic pentagon code yields a matchgate tensor on the boundary (see Fig. 2). The explicit construction is given in the Supplementary Materials. Using the Schläfli symbol  $\{p, q\}$ , where  $p$  is the number of edges per polygon and  $q$  is the number of polygons around each corner, we can specify the hyperbolic geometry of the HaPPY model as a regular  $\{5, 4\}$  tiling.

We find that the correlation structure of this model is best captured in the Majorana picture. Explicitly, consider the pentagon tiling of  $(12)$  with all bulk inputs set to the positive-parity eigenvector  $|\bar{0}\rangle$ . The entries of the Majorana covariance matrix  $\Gamma_{j,k} = \frac{1}{2}\langle \Psi | [\gamma_j, \gamma_k] | \Psi \rangle$  resulting from successive contraction steps are shown in Fig. 3 (A to C). As

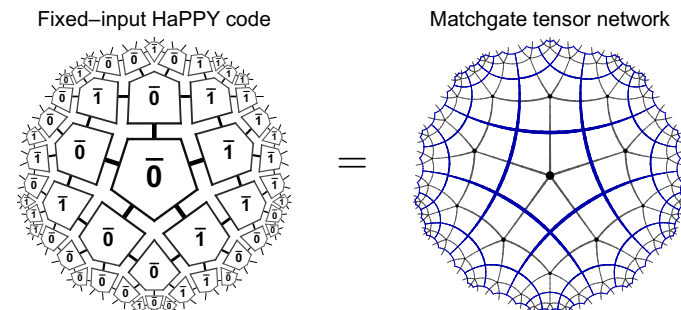


**Fig. 2. HaPPY/matchgate equivalence.** The holographic pentagon code of the HaPPY model for fixed computational bulk input (left) is equal to a matchgate tensor network on a hyperbolic pentagon tiling (right).

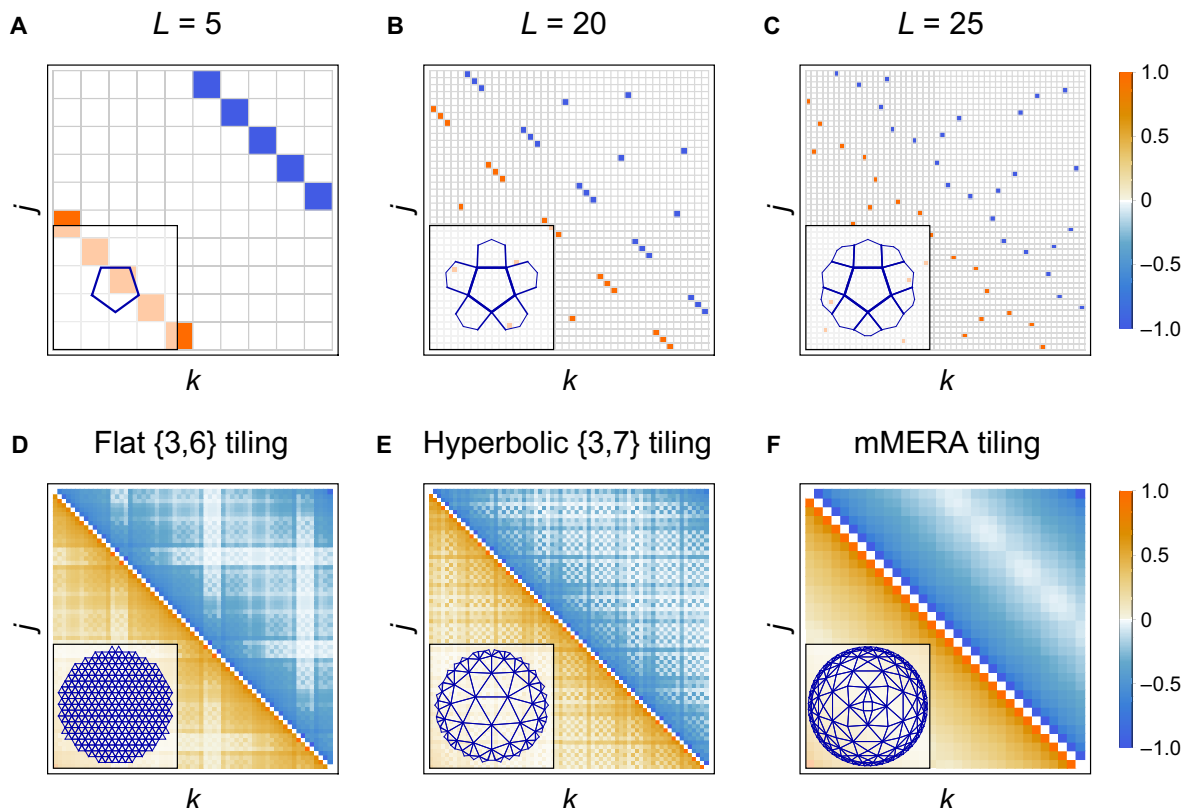


**Fig. 3. Boundary state correlations.** (A to C) Majorana covariance matrix  $\Gamma$  with color-coded entries for a boundary state of a hyperbolic  $\{5,4\}$  tiling of the HaPPY code with fixed  $\bar{0}$  input on each tile. Boundary consists of  $2L = 10, 40,$  and  $50$  Majorana sites, respectively. (D to F) Field correlation matrix  $\langle \Psi_j | \Psi_k - \Psi_k | \Psi_j \rangle / 2 = (\Gamma_{2j,2k-1} + \Gamma_{2j-1,2k}) / 4$  for boundary states of the  $\{3,6\}, \{3,7\},$  and mMERA tiling at criticality with  $L = 63, 69,$  and  $64$  boundary sites, respectively. Matrix entries are normalized to the same color scale. The tiling corresponding to each correlation matrix in (A) to (F) is shown in the lower left corner.

we can see, both the individual pentagon state and the larger contracted states are characterized by a nonlocal pairing of Majorana fermions. The contractions effectively connect Majorana pairs from each pentagon to a larger chain, so the pairs on the boundary of the contracted network can be seen as end points of a discretized “geodesic” spanning the bulk. While this discontinuous correlation pattern of  $\Gamma_{j,k}$  makes the computation of CFT observables difficult, we can estimate the average correlation falloff by counting the relative frequency  $n(d)$  of Majorana pairs at distance  $d = |j - k|$  over which they connect points on the boundary. According to the results shown in Fig. 4A, correlation falloff follows a power law  $n(d) \propto d^{-1}$ , as expected of a CFT. Furthermore, we compute the entanglement entropy  $S_A$  of a subsystem  $A$  of size  $l$  averaged over all boundary positions, defined as

$$\mathbb{E}_l(S) = \sum_{k=1}^L S_{[k,k+l]} \tag{10}$$

The result, shown in Fig. 4B, closely follows the Calabrese-Cardy formula for periodic 1 + 1-dimensional CFTs, given by (33, 34)

$$S_A = \frac{c}{3} \log \left( \frac{L}{\pi \epsilon} \sin \frac{\pi l}{L} \right) \approx \frac{c}{3} \log \frac{l}{\epsilon} + O((l/L)^2) \tag{11}$$

with a numerical fit yielding  $c \approx 4.2$  and  $\epsilon \approx 1.1$  for a cutoff at  $L = 2605$  boundary sites.

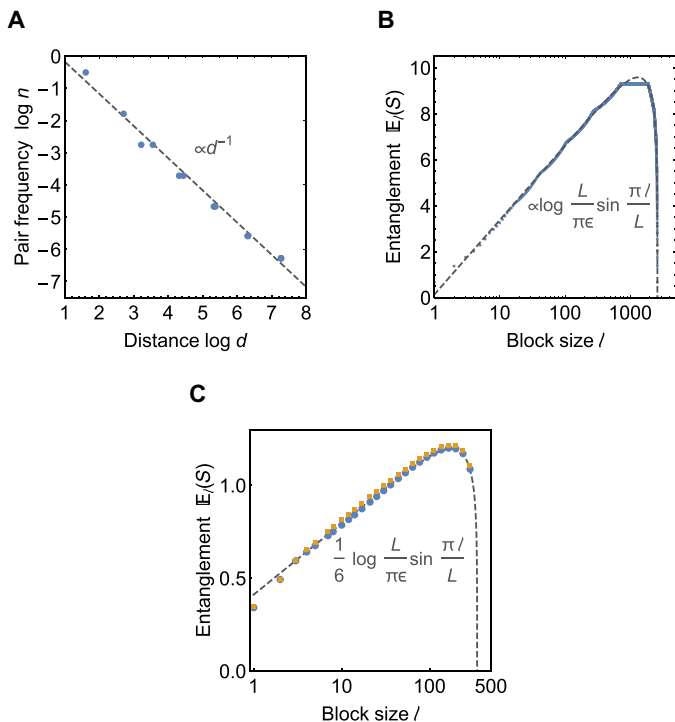


**Fig. 4. Critical correlations and entanglement scaling.** (A and B) Boundary state properties of the HaPPY code at 2605 boundary sites. (A) shows average correlations at boundary distance  $d$ , computed as the relative frequency  $n$  of Majorana pairs. Dashed gray line shows a  $n(d) \sim 1/d$  numerical fit. (B) shows the scaling of average entanglement entropy  $\mathbb{E}_l(S)$  with subsystem size  $l$ . Dashed gray line shows numerical fit using (11). (C)  $\mathbb{E}_l(S)$  for regular tilings at the critical values  $a = 0.580$  for a  $\{3,6\}$  tiling (blue) and at  $a = 0.609$  for the  $\{3,7\}$  tiling (yellow) with 348 boundary sites each. The dashed gray line shows the exact  $c = 1/2$  CFT solution.

The peculiar pairwise correlation of boundary Majorana modes, suggesting a connection to Majorana dimer models (35), is more deeply explored in a separate publication (36). However, as the correlation structure breaks the translation and scale invariance expected of CFT ground states, we now consider regular tilings with generic matchgate input.

**Regular triangulations**

As the boundary states of triangular tilings are necessarily Gaussian (15), we can study their properties comprehensively using matchgate tensors. The simplest such tilings are regular and isotropic, i.e., with each local tensor specified by the same antisymmetric  $3 \times 3$ -generating matrix  $A$ . Isotropy constrains its components to one parameter  $a = A_{1,2} = A_{1,3} = A_{2,3}$ . The bulk topology follows from our choice of tiling. For triangular tilings ( $p = 3$ ), setting  $q = 6$  produces a flat tiling, whereas  $q > 6$  leads to a hyperbolic one (see Fig. 1, A and B). Triangular tilings with  $q < 6$  produce closed polyhedra that are positively curved and lack the notion of an asymptotic boundary. As a convention, we choose the local orientation of the triangles so that the generating matrix for the contracted boundary state satisfies  $A'_{ij} > 0$  for  $i > j$ , corresponding to antiperiodic boundary conditions: Covariance matrix entries  $\Gamma_{i,j}$  acquire a sign flip when cyclic permutations push either index  $i$  or  $j$  over the boundary, as relative ordering is reversed.

We now consider the boundary states of  $\{3, k\}$  bulk tilings. The falloff of correlations along the boundary generally depends on  $k$ , i.e., the bulk curvature, as shown in Fig. 5 (A and B) for the  $a = 0.25$  case. While correlations between the boundary Majorana fermions of a flat bulk fall off exponentially, a hyperbolic bulk produces a polynomial decay (up to

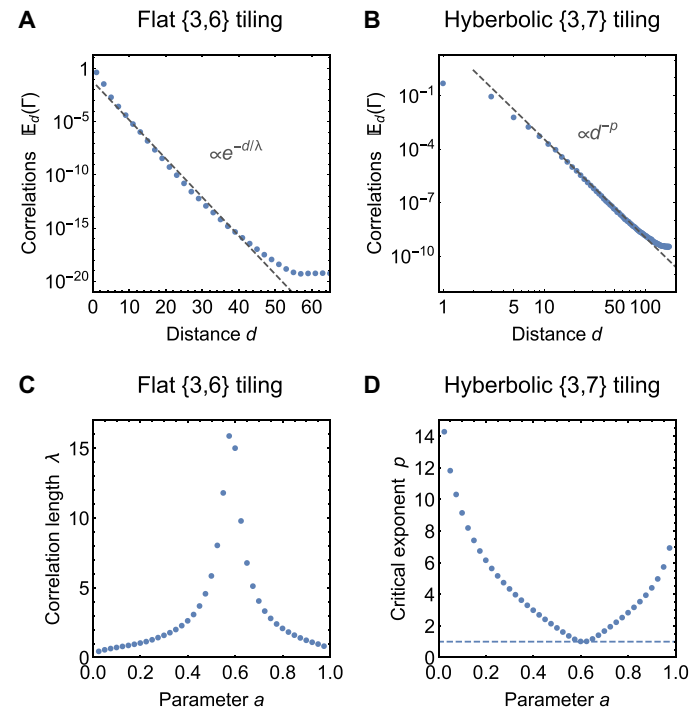


**Fig. 5. Boundary correlations for regular tilings.** (A and B) Mean value of Majorana covariance  $\mathbb{E}_d(\Gamma) = \sum_{k=1}^L |\Gamma_{k,k+d}| / L$  (with  $\Gamma_{i,L+j} = \Gamma_{ij}$ ) at boundary distance  $d$ . For  $\{3,6\}$  tiling with 150 boundary Majorana fermions (left) and  $\{3,7\}$  tiling with 348 (right).  $a = 0.25$  in both cases. (C and D) Dependence of correlation falloff on  $a$  for  $\{3,6\}$  tiling with falloff  $\sim e^{-d/\lambda}$  (left) and  $\{3,7\}$  tiling with  $\propto d^{-p}$  (right).

Downloaded from <http://advances.sciencemag.org/> on September 5, 2019

finite-size effects at large distances and rounding errors at very small correlations). In the hyperbolic case, geodesics between boundary points scale logarithmically in boundary distance, so the falloff is still exponential in bulk distance, as we would expect in AdS/CFT (37).

Restricting ourselves to the  $0 < a < 1$  region, we explore how quickly correlations decay in both settings. At  $a = 0$  and  $a = 1$ , the boundary Majorana fermions only have neighboring pair correlations, either pairing within each edge ( $a = 0$ ) or across the corners ( $a = 1$ ). Thus, correlation decay becomes infinite in the limits  $a \rightarrow 0$  and  $a \rightarrow 1$ , independent of bulk geometry. We use numerical fits to study the remaining region  $0 < a < 1$  (see Fig. 5, C and D). For a hyperbolic bulk geometry, the power law is generic with the slowest decay at  $a \approx 0.61$ , where we see a  $\propto d^{-1}$  falloff over distance  $d$ . The exponential decay  $\propto e^{-d/\lambda}$  generally produced by a flat bulk geometry, however, slows down to a power law (with correlation length  $\lambda$  diverging) around  $a \approx 0.58$ , where correlations again decay as  $\propto d^{-1}$ . At their critical values, the boundary states of both bulk geometries have the same average properties.

Up to finite-size effects, this critical boundary theory turns out to be the Ising CFT, as we confirm by computing a range of critical properties from the covariance matrix, shown in Table 1. The entanglement entropy scaling, shown in Fig. 4C, again matches the expected form (11) irrespective of the choice of tiling. The Ising CFT state that we observe at the critical value of  $a$  is the ground state of the Hamiltonian

$$H = i \left( \sum_{k=1}^{N-1} \gamma_k \gamma_{k+1} + \gamma_1 \gamma_N \right) \quad (12)$$

where the sign of the boundary term  $\gamma_1 \gamma_N$  signifies antiperiodic boundary conditions. Triangular tilings also incorporate more generic models: By associating each edge with a bond dimension  $\chi > 2$ , it is possible to produce boundary theories with central charges  $c$  larger than  $1/2$ . In the simplest case, we choose a generating matrix that only couples between sets of fermionic modes, resulting in a boundary theory that consists of multiple copies of the Ising CFT and a corresponding central charge that is a multiple of  $1/2$  (note that this construction is only possible for  $\{n, k\}$  tilings with even  $k$ ). Furthermore, by changing the tensor content in a central region of the network, a mass gap can be introduced, highlighting how radii in a hyperbolic bulk correspond to a re-

normalization scale on the boundary. Details are provided in the Supplementary Materials.

### Translation invariance and MERA

The regular bulk tilings considered so far have a set of discrete symmetries. When choosing identical tensors on each polygon, the boundary states necessarily inherit these symmetries, breaking translation invariance. To recover it, we consider a tiling with the same geometry as the MERA network. As we restrict ourselves to real generating matrices for the three- and four-leg matchgate tensors in this geometry, our model is not a unitary circuit but a model of Euclidean entanglement renormalization resembling imaginary time evolution, extending ideas from (19, 20). This may provide a more realistic representation of the causal structure of an AdS time slice than the standard MERA. Accordingly, the tensors of our matchgate MERA (mMERA) do not correspond to the usual (norm-preserving) isometries and disentglers. We can still produce almost perfectly translation-invariant boundary states (Fig. 3F) while optimizing over only three parameters and recover the expected CFT properties (Table 1). In particular, at bond dimension  $\chi = 2$ , the ground-state energy has a relative error of only 0.02% compared to the exact solution. Note that the optimization process only takes a few minutes on a desktop computer for a network with hundreds of tensors. We also find that the  $\chi = 2$  mMERA has a symmetry that allows us to write its four-leg tensors as contractions of simpler three-leg tensors (see Fig. 1C), yielding a nonregular triangular tiling. An interesting question to pursue is whether alternating or quasiperiodic tilings with a larger parameter space than regular tilings can also produce translation-invariant states.

### DISCUSSION

In this work, we have studied bulk-boundary correspondences in fermionic Gaussian tensor networks, introducing a versatile framework and a highly efficient contraction method based on matchgate tensors (14, 15) for a wide class of flat and hyperbolic bulk tilings. We showed that our framework includes the holographic pentagon code built from five-qubit stabilizer states for fixed bulk inputs. Its boundary states correspond to a nonlocal bulk pairing of Majorana fermions, opening an avenue to studying the state properties of this holographic model at large sizes. We explicitly computed two-point correlators and entanglement entropies, which were found to exhibit critical scaling. Beyond known models, we showed that critical and gapped Gaussian boundary states can be realized by various bulk tilings. In particular, the average scaling properties of the  $c = 1/2$  Ising CFT (and multiples thereof) can be reproduced using regular one-parameter bulk triangulations with both flat and hyperbolic curvature. This is particularly unexpected for the flat case where boundary theories are typically gapped and raises the question whether this appearance of criticality is retained in strongly interacting models as well. The appearance of equivalent boundary CFT states for flat and hyperbolic bulks resembles the effect of local Weyl transformations in Euclidean path integrals (38). Our reproduction of conformal properties from an isotropic tensor network with only a single parameter further suggests that isotropy is a powerful symmetry for numerical CFT computations. Furthermore, we constructed the mMERA, a Euclidean matchgate tensor network based on the MERA geometry. Beyond the results achievable with regular triangulations, this tiling, which can also be expressed as a triangulation, recovers the Ising CFT with translation invariance while requiring only three free parameters and little computational cost.

**Table 1. Table of conformal data for the regular {3, 6} and {3, 7} bulk tilings as well as the mMERA, compared to the exact results and the wavelet MERA (16).** Listed are the ground-state energy density  $\epsilon_0$ , central charge  $c$ , scaling dimensions  $\Delta_\phi$  of the fields  $\phi = \psi, \bar{\psi}, \epsilon, \sigma$ , and the structure constant  $C_{\sigma, \sigma, \epsilon}$ . The nonscaling of the identity  $\mathbb{1}$  is discussed in the Supplementary Materials.

	Exact	{3, 6} bulk	{3, 7} bulk	mMERA	Wavelets
$\epsilon_0$	-0.6366	-0.6139	-0.5617	-0.6365	-0.6211
$c$	0.5000	0.5006	0.5018	0.4958	0.4957
$\Delta_\psi, \Delta_{\bar{\psi}}$	0.5000	0.4948	0.4951	0.5023	0.5000
$\Delta_\epsilon$	1.0000	0.9856	1.0121	1.0027	1.0000
$\Delta_\sigma$	0.1250	0.1403	0.1368	0.1417	0.1402
$C_{\sigma, \sigma, \epsilon}$	0.5000	0.5470	0.5336	0.5156	0.4584

Within the Gaussian setting, further studies could focus on positively curved bulks, higher-dimensional models, and random tensors. Beyond Gaussianity, one could also explore interacting fermionic tensor networks (39–43) by a weak-coupling expansion or under locally restricted interactions. Both of these possible extensions to our framework would require computations scaling only polynomially in the system size, thus still avoiding the prohibitive computational effort of general methods for exact tensor contraction.

## SUPPLEMENTARY MATERIALS

Supplementary material for this article is available at <http://advances.sciencemag.org/cgi/content/full/5/8/eaaw0092/DC1>

Section S1. Tensor contractions in the Grassmann formalism

Section S2. Matchgates and fermionic Gaussian states

Section S3. Conversion of generating matrices to covariance matrices

Section S4. Contraction rules for generating matrices

Section S5. Explicit generating matrices and numerical results

Fig. S1. Combining tiles of matchgates.

Fig. S2. Tile orientations under contraction.

Fig. S3. Constructing the mMERA.

Fig. S4. Energy convergence of the mMERA.

Fig. S5. Determining scaling dimensions of flat tilings.

Fig. S6. Determining scaling dimensions of hyperbolic tilings.

Fig. S7. Determining scaling dimensions of mMERA.

Fig. S8. Determining structure constants.

Fig. S9. Correlations and entanglement with IR cutoff.

Fig. S10. Construction of triangle states with bond dimension  $\chi = 2, 4, 8$ .

Table S1. Values of the critical generating matrix parameter  $a$  for different  $(3, k)$  triangular tilings and ultraviolet cutoffs.

Table S2. Exact conformal scaling dimension of various (quasi-)primary fields  $\phi$  of the Ising CFT.

References (44–51)

## REFERENCES AND NOTES

- J. M. Maldacena, The large  $N$  limit of superconformal field theories and supergravity. *Adv. Theor. Math. Phys.* **2**, 231–252 (1998).
- M. Van Raamsdonk, Building up spacetime with quantum entanglement. *Gen. Rel. Grav.* **42**, 2323–2329 (2010).
- F. Pastawski, J. Preskill, Code properties from holographic geometries. *Phys. Rev. X* **7**, 021022 (2017).
- J. Eisert, M. Cramer, M. B. Plenio, *Colloquium: Area laws for the entanglement entropy*. *Rev. Mod. Phys.* **82**, 277–306 (2010).
- S. Ryu, T. Takayanagi, Holographic derivation of entanglement entropy from the anti-de Sitter space/conformal field theory correspondence. *Phys. Rev. Lett.* **96**, 181602 (2006).
- B. G. Swingle, Entanglement renormalization and holography. *Phys. Rev. D* **86**, 065007 (2012).
- G. Vidal, Class of quantum many-body states that can be efficiently simulated. *Phys. Rev. Lett.* **101**, 110501 (2008).
- G. Evenbly, G. Vidal, Algorithms for entanglement renormalization. *Phys. Rev. B* **79**, 144108 (2009).
- C. M. Dawson, J. Eisert, T. J. Osborne, Unifying variational methods for simulating quantum many-body systems. *Phys. Rev. Lett.* **100**, 130501 (2008).
- A. Almheiri, X. Dong, D. Harlow, Bulk locality and quantum error correction in AdS/CFT. *J. High Energy Phys.* **1504**, 163 (2015).
- C. H. Lee, X.-L. Qi, Exact holographic mapping in free fermion systems. *Phys. Rev. B* **93**, 035112 (2016).
- F. Pastawski, B. Yoshida, D. Harlow, J. Preskill, Holographic quantum error-correcting codes: Toy models for the bulk/boundary correspondence. *J. High Energy Phys.* **2015**, 149 (2015).
- P. Hayden, S. Nezami, X.-L. Qi, N. Thomas, M. Walter, Z. Yang, Holographic duality from random tensor networks. *J. High Energy Phys.* **2016**, 9 (2016).
- L. G. Valiant, Quantum circuits that can be simulated classically in polynomial time. *SIAM J. Comput.* **31**, 1229–1254 (2002).
- S. Bravyi, Contraction of matchgate tensor networks on non-planar graphs. *Cont. Math.* **482**, 179–211 (2009).
- G. Evenbly, S. R. White, Entanglement renormalization and wavelets. *Phys. Rev. Lett.* **116**, 140403 (2016).
- J. Haegeman, B. Swingle, M. Walter, J. Cotler, G. Evenbly, V. B. Scholz, Rigorous free fermion entanglement renormalization from wavelet theory. *Phys. Rev. X* **8**, 011003 (2018).
- G. Evenbly, Hyperinvariant tensor networks and holography. *Phys. Rev. Lett.* **119**, 141602 (2017).
- G. Evenbly, G. Vidal, Tensor network renormalization. *Phys. Rev. Lett.* **115**, 180405 (2015).
- G. Evenbly, G. Vidal, Tensor network renormalization yields the multiscale entanglement renormalization ansatz. *Phys. Rev. Lett.* **115**, 200401 (2015).
- R. Orus, A practical introduction to tensor networks: Matrix product states and projected entangled pair states. *Ann. Phys.* **349**, 117–158 (2014).
- N. Schuch, *Lecture notes for the 44th IFF Spring School “Quantum Information Processing” in Juelich* (2013).
- F. Verstraete, J. I. Cirac, V. Murg, Matrix product states, projected entangled pair states, and variational renormalization group methods for quantum spin systems. *Adv. Phys.* **57**, 143–224 (2008).
- J. Eisert, Entanglement and tensor network states. *Mod. Sim.* **3**, 520 (2013).
- F. A. Berezin, *The Method of Second Quantization* (Academic Press, 1966).
- K. E. Cahill, R. J. Glauber, Density operators for fermions. *Phys. Rev. A* **A59**, 1538–1555 (1999).
- S. Bravyi, Lagrangian representation for fermionic linear optics. *Quantum Inf. Comput.* **5**, 216–238 (2005).
- B. M. Terhal, D. P. DiVincenzo, Classical simulation of noninteracting-fermion quantum circuits. *Phys. Rev. A* **65**, 032325 (2002).
- R. Laflamme, C. Miquel, J. P. Paz, W. H. Zurek, Perfect quantum error correcting code. *Phys. Rev. Lett.* **77**, 198–201 (1996).
- D. Gottesman, Class of quantum error-correcting codes saturating the quantum hamming bound. *Phys. Rev. A* **54**, 1862–1868 (1996).
- B. M. Terhal, Quantum error correction for quantum memories. *Rev. Mod. Phys.* **87**, 307–346 (2015).
- D. Gottesman, “Stabilizer codes and quantum error correction,” thesis, California Institute of Technology (1997).
- C. Holzhey, F. Larsen, F. Wilczek, Geometric and renormalized entropy in conformal field theory. *Nucl. Phys. B* **B424**, 443–467 (1994).
- P. Calabrese, J. Cardy, Entanglement entropy and quantum field theory. *J. Stat. Mech.* **0406**, P06002 (2004).
- B. Ware, J. H. Son, M. Cheng, R. V. Mishmash, J. Alicea, B. Bauer, Ising anyons in frustration-free majorana-dimer models. *Phys. Rev. B* **94**, 115127 (2016).
- A. Jahn, M. Gluza, F. Pastawski, J. Eisert, Majorana dimers and holographic quantum error-correcting codes, arXiv:1905.03268 [hep-th] (8 May 2019).
- V. Balasubramanian, S. F. Ross, Holographic particle detection. *Phys. Rev.* **D61**, 044007 (2000).
- P. Caputa, N. Kundu, M. Miyaji, T. Takayanagi, K. Watanabe, Anti-de Sitter space from optimization of path integrals in conformal field theories. *Phys. Rev. Lett.* **119**, 071602 (2017).
- T. Barthel, C. Pineda, J. Eisert, Contraction of fermionic operator circuits and the simulation of strongly correlated fermions. *Phys. Rev. A* **80**, 042333 (2009).
- P. Corboz, R. Orus, B. Bauer, G. Vidal, Simulation of strongly correlated fermions in two spatial dimensions with fermionic projected entangled-pair states. *Phys. Rev. B* **81**, 165104 (2010).
- C. V. Kraus, N. Schuch, F. Verstraete, J. I. Cirac, Fermionic projected entangled pair states. *Phys. Rev. A* **81**, 052338 (2010).
- C. Wille, O. Buerschaper, J. Eisert, Fermionic topological quantum states as tensor networks. *Phys. Rev. B* **95**, 245127 (2017).
- N. Bultinck, D. J. Williamson, J. Haegeman, F. Verstraete, Fermionic matrix product states and one-dimensional topological phases. *Phys. Rev. B* **95**, 075108 (2017).
- H. N. V. Temperley, M. E. Fisher, Dimer problem in statistical mechanics—an exact result. *Phil. Mag.* **6**, 1061–1063 (1961).
- P. W. Kasteleyn, The statistics of dimers on a lattice: I. The number of dimer arrangements on a quadratic lattice. *Phys. Ther.* **27**, 1209–1225 (1961).
- J.-Y. Cai, V. Choudhary, P. Lu, On the theory of matchgate computations, in *Twenty-Second Annual IEEE Conference on Computational Complexity (CCC’07)* (IEEE, 2007), pp. 305–318.
- C. Bloch, A. Messiah, The canonical form of an antisymmetric tensor and its application to the theory of superconductivity. *Nucl. Phys.* **39**, 95–106 (1962).
- C. V. Kraus, “A quantum information perspective of fermionic quantum many-body systems,” thesis, Universität München (2009).
- S. Bravyi, D. Gosset, Complexity of quantum impurity problems. *Comm. Math. Phys.* **356**, 451–500 (2016).
- P. Francesco, P. Mathieu, D. Sénéchal, *Conformal Field Theory* (Springer, 1997).
- A. Serafini, F. Illuminati, S. De Siena, Von Neumann entropy, mutual information and total correlations of Gaussian states. *J. Phys.* **B37**, L21 (2004).

**Acknowledgments:** We would like to thank A. Kubica for pointing out that  $[[5,1,3]]$  code states (29) are ground states of quadratic Majorana Hamiltonians. We also thank X.-L. Qi, T. Takayanagi, and P. Caputa for helpful discussions. **Funding:** We thank the ERC (TAQ), the DFG (CRC 183, EI 519/7-1, EI 519/14-1, and EI 519/15-1), the John Templeton Foundation, the EC (PASQuanS), the Studienstiftung, and the Alexander von Humboldt Foundation for support. **Author contributions:** F.P. and J.E. conceived the project and provided guidance, while A.J. and M.G. performed analytical calculations. A.J. provided the numerical computations and figure design. All authors discussed the results and wrote the manuscript. **Competing interests:** The authors declare that they have no competing interests. F.P. is currently employed by Psi Quantum Inc. but provided his main contribution to this work while being employed at Freie Universität Berlin. **Data and materials**

**availability:** All data needed to evaluate the conclusions in the paper are present in the paper and/or the Supplementary Materials. All data related to this paper may be requested from the authors.

Submitted 13 November 2018

Accepted 28 June 2019

Published 9 August 2019

10.1126/sciadv.aaw0092

**Citation:** A. Jahn, M. Gluzn, F. Pastawski, J. Eisert, Holography and criticality in matchgate tensor networks. *Sci. Adv.* **5**, eaaw0092 (2019).

## Holography and criticality in matchgate tensor networks

A. Jahn, M. Gluza, F. Pastawski and J. Eisert

*Sci Adv* 5 (8), eaaw0092.

DOI: 10.1126/sciadv.aaw0092

### ARTICLE TOOLS

<http://advances.sciencemag.org/content/5/8/eaaw0092>

### SUPPLEMENTARY MATERIALS

<http://advances.sciencemag.org/content/suppl/2019/08/05/5.8.eaaw0092.DC1>

### REFERENCES

This article cites 44 articles, 0 of which you can access for free  
<http://advances.sciencemag.org/content/5/8/eaaw0092#BIBL>

### PERMISSIONS

<http://www.sciencemag.org/help/reprints-and-permissions>

Use of this article is subject to the [Terms of Service](#)

---

*Science Advances* (ISSN 2375-2548) is published by the American Association for the Advancement of Science, 1200 New York Avenue NW, Washington, DC 20005. 2017 © The Authors, some rights reserved; exclusive licensee American Association for the Advancement of Science. No claim to original U.S. Government Works. The title *Science Advances* is a registered trademark of AAAS.